Science Advances

AAAS

advances.sciencemag.org/cgi/content/full/4/1/eaap8294/DC1

Supplementary Materials for

Thin films of topological Kondo insulator candidate SmB_6: Strong spin-orbit torque without exclusive surface conduction

Yufan Li, Qinli Ma, S. X. Huang, C. L. Chien

Published 19 January 2018, *Sci. Adv.* **4**, eaap8294 (2018)
DOI: 10.1126/sciadv.aap8294

This PDF file includes:

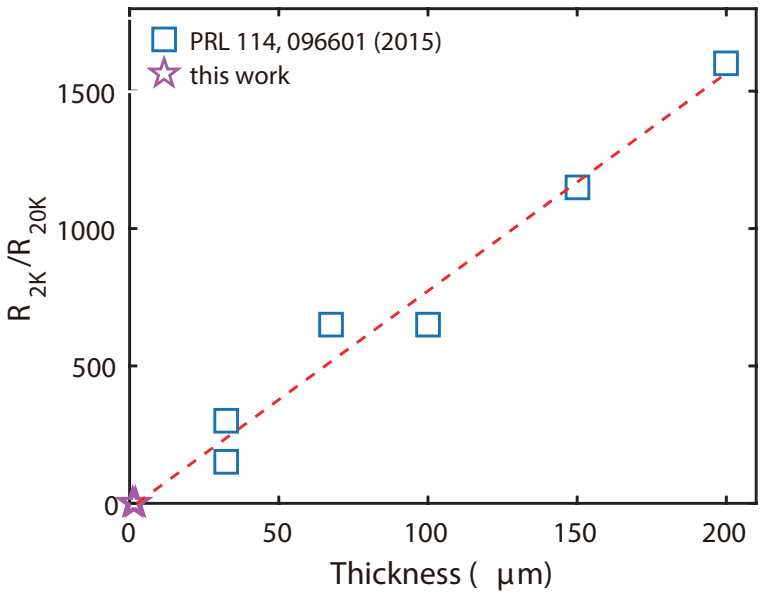

fig. S1. Resistance ratio R_{2K}/R_{20K} as a function of sample thicknesses. The blue squares are reproduced from PRL 114, 096601 (2015) [35]. The red dashed line is the linear fitting to the blue squares. The pink pentagram represents the result from this work.

section S1. Comparison of the transport properties of SmB_6 thin films and single-crystal bulk specimens

In the manuscript we demonstrated experimental observations in thin films that are in apparent contradiction to the 2D transport features concluded by studies using bulk specimens. An intriguing question that follows is whether any convergence can be found in the transport properties between thin film samples and single-crystal bulk specimens. One major difference between the bulk samples and the thin film samples is that in bulk specimen the resistance changes by 10^3 ~ 10^5 times from room temperature down to below 10 K, whereas in thin films it only changes by about 30 %. However, we note that Syers *et al.* [35] studied single-crystal bulk samples with thicknesses ranged from 200 μm to 32.5 μm. Even at these macroscopic thicknesses, the ratio R_{2K}/R_{20K} decreases rapidly from 1600 for 200 μm-thick sample to 200 ~ 300 for 32.5 μm-thick sample. In fig. S1, we plot the R_{2K}/R_{20K} values obtained from their bulk single crystals together with the R_{2K}/R_{20K} values of our thin films (1.06 ~ 1.07 for all thicknesses). Very interestingly, the R_{2K}/R_{20K} values of our thin films are consistent with those of the bulk crystals that decrease linearly with reduced thickness.

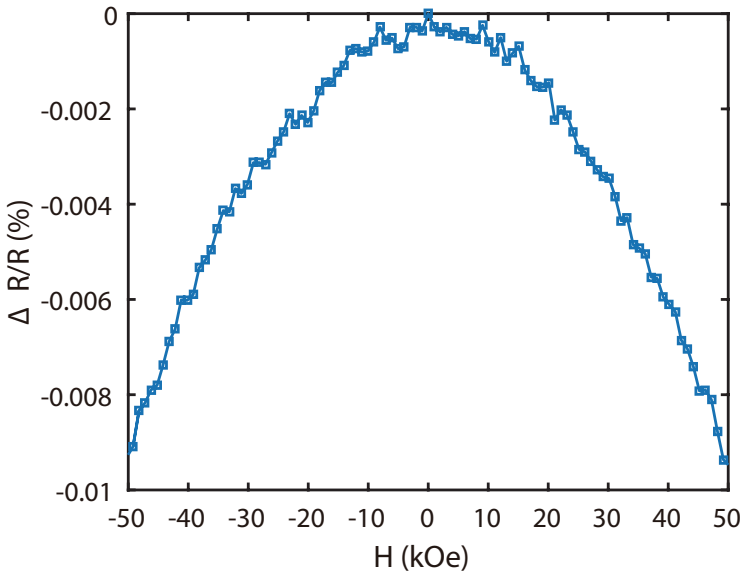

fig. S2. Magnetoresistance of SmB_6 thin films. The longitudinal magnetoresistance of the 250 nm-thick film obtained at 1.8 K.

In the manuscript we also show that the activation energy of the thin films is consistent with the reported values in bulk samples. This implies that the hybridization gap in the thin films is the same as the bulk materials. These are evidences that the transport properties of thin-film samples and single-crystal samples may converge when they have similar thicknesses.

section S2. Magneto-resistance and Hall effect

The SmB_6 thin films display a negative magneto-resistance (MR) at 2 K, in agreement with bulk specimen [43]. A representative MR curve is shown in fig. S2, obtained from a 250 nm-thick film.

In fig. S3, we show the Hall resistance versus field curves for 3 representative film thicknesses at 3 characteristic temperatures. Evidently, all the field dependences (R_{yx} vs. H) are very linear, with only small deviations from linear fitting, presumably due to possible multi-type carriers. We found our Hall effect results in qualitative agreement with that reported in sputtered polycrystalline SmB_x films [44].

section S3. Additional data on crystalline and chemical stoichiometry characterizations

In fig. S4, we show the XRD patterns for our films samples with the thicknesses ranging from 50 nm to 500 nm. The FWHM of thicker films (250 nm and 500 nm) is about 0.8°, while broader for thinner films (50 nm and 100 nm) at around 1.4°. This is expected due to

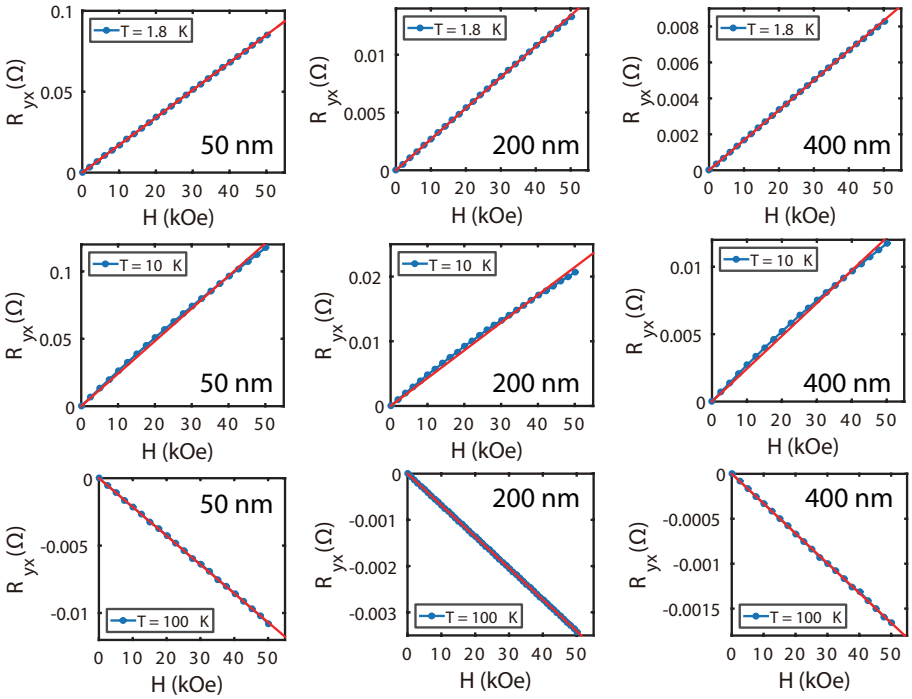

fig. S3. Hall resistance of SmB_6 thin films. Hall resistance as a function of magnetic field for 50 nm, 200 nm, 400 nm thick films measured at 1.8 K, 10 K, 100 K respectively.

smaller thickness. For all films, the surface is composed of only the SmB_6 (100) plane; no other phases are observed. This is the crystal plane on which the topological surface state (TSS) is proposed to reside. Therefore our samples should be able to evidence the TSS, should it be present.

X-ray photoelectron spectroscopy (XPS) was employed to verify the stoichiometry of SmB_6. A full spectrum is shown in fig. S5. The carbon and oxygen peaks are due to the absorption from exposure to the air, and can be removed or suppressed after slight Ar^+ bombardment at the surface. Fine scans were performed to Sm $3d^5$ and B 1s peaks, carried out on a 500 nm-thick thin film and a polycrystalline bulk specimen cut from stoichiometric target, while the latter is used for calibrating the measured chemical composition. We obtain the atomic ratio $r_{B:Sm}$ for our sputtered thin film as 5.90±0.11.

section S4. SOT-induced switching of perpendicularly magnetized CoFeB

In fig. S6, more experimental data of the SOT-induced switching on CoFeB(1)/W(0.8)/SmB_6(t) samples were provided. All switching curves were measured under the same external in-plane field of 200 Oe, parallel or anti-parallel to the current direction. The film thickness of SmB_6 and the temperature at which the measurements were carried out are denoted on the

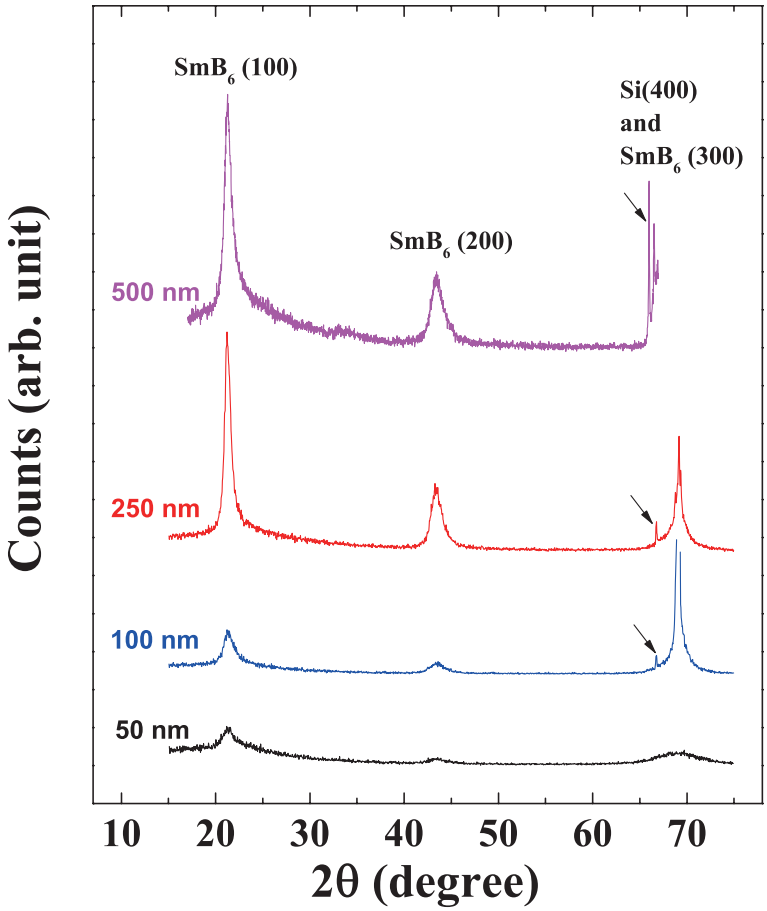

fig. S4. Additional XRD data of SmB_6 thin films. XRD scan of the SmB_6 / Si(001) thin films with various film thicknesses. Some impurity phase from silicon substrate is also visible (marked by black arrows).

figures.

section S5. Current distribution in multilayer thin films

The SOT-induced switching experiments involve devices comprised of metallic multilayer structure. It is important to consider the current distribution in different layers in order to evaluate the SOT contributed by SmB_6 and/or β–W. In our experiment, control samples of magnetic trilayer without SmB_6 were deposited on bare Si substrate side-by-side with the samples with SmB_6 underlayers. The sheet resistance of the trilayer MgO(1.5)/CFB(1)/W(0.8) were henceforth determined to be 1250 Ω/□ and the anomalous Hall resistance about 12 Ω. Two methods are employed to independently quantify the current distribution through the SmB_6 layer and the trilayer. Firstly the current distribution can be assessed using the two-conductor-in-parallel model, which apparently gives $I_{SmB_6}R_{SmB_6} = I_{trilayer}R_{trilayer}$. The result is shown as the dashed line in Fig. 3c of the

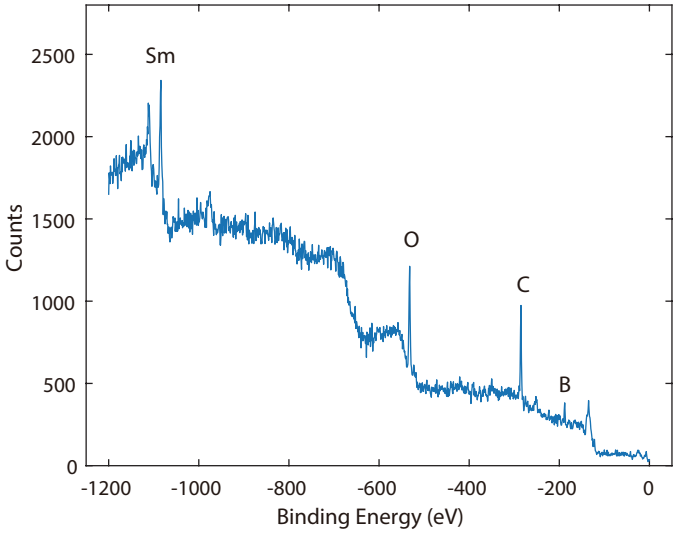

fig. S5. XPS spectrum of SmB_6 thin films. XPS spectrum of 500 nm-thick SmB_6 / Si(001) thin film. The sample was exposed to ambient atmosphere before transferred into vacuum and measured as is.

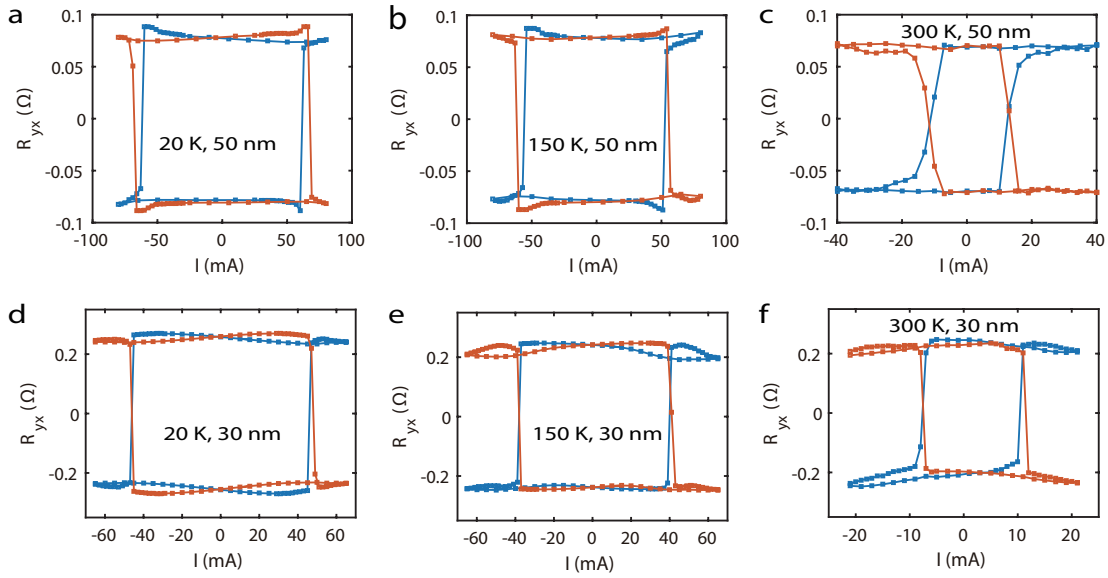

fig. S6. Additional SOT switching results of various temperatures.
The SOT-induced switching measurement of samples with SmB_6 thickness as 50 nm (**a**, **b**, and **c**) and 30 nm (**d**, **e**, and **f**). External in-plane field, 200 Oe (blue curves) and -200 Oe (red curves) was applied along the current direction. Pulsed current of 12 ms width and amplitude plotted as the x axis was applied to induce switching, followed by a small probing DC current of 0.5 mA for measuring R_{yx}.

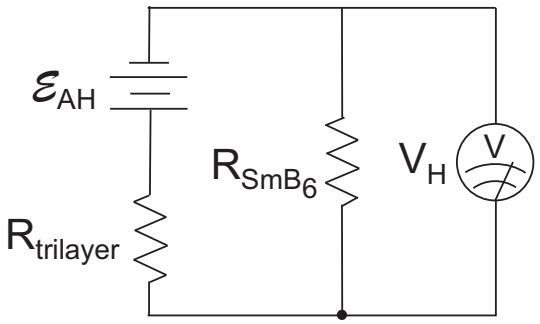

fig. S7. A schematic diagram of the anomalous Hall voltage measurement under the presence of a nonmagnetic shunting layer. The equivalent diagram of experimental Hall voltage measurement under the presence of a non-magnetic shunting layer SmB_6.

manuscript. The resistivity of SmB_6 is taken as 600 $\mu\Omega cm$, as determined from fitting the thickness-dependent resistance, as shown in Fig. 2. The other approach is through the shunting effect of anomalous Hall voltage caused by the non-magnetic SmB_6 layer. The principle is depicted in fig. S7, where $\mathscr{E}_{AH}$ is the anomalous Hall voltage generated in the trilayer by $I_{trilayer}$, and V_H is the Hall voltage across the multilayer device that can be measured experimentally. Taken into account that the Hall resistance of the multilayer device is defined as $R_H = V_H/I_{tot} = V_H/(I_{trilayer} + I_{SmB_6})$, one arrives at $I_{trilayer}/I_{tot} = (R_H/R_H^{trilayer})^{1/2}$. The results for different SmB_6 are shown in Fig. 3c as discrete points. The results from two independent methods agree well. We conclude that the second approach is somewhat superior, as it is immune to possible deviation of the actual SmB_6 film thickness from the expected value, which would otherwise result experimental error in determining R_{SmB_6} in the first approach. Therefore, the result from the second method was used in further quantitative analyses regarding the SOT-induced switching, as described in the manuscript.

In fig. S8a we show the temperature dependence of the sheet resistance of pristine 50 nm-thick SmB_6 thin film and the magnetic trilayer. Both has little variation from room temperature down to cryogenic temperatures. As a result, I_{SmB_6}/I_{tot} has very small temperature variation of only about 1%, as shown in fig. S8b.

In order to compare the critical switching current density of β–W and SmB_6, the current distribution between W and CFB also need to be resolved. Fig. S9 shows the sheet resistance of CFB(1)/W(t), where t varies as in a thickness wedge of the W layer. The thickness-dependent sheet resistance is fitted using $R\Box = t_W^{-1}\rho_W \cdot t_{CFB}^{-1}\rho_{CFB}/(t_W^{-1}\rho_W + t_{CFB}^{-1}\rho_{CFB})$. We obtain ρ_W as 265 $\mu\Omega cm$ and ρ_{CFB} as 114 $\mu\Omega cm$, in good agreement with previously reported

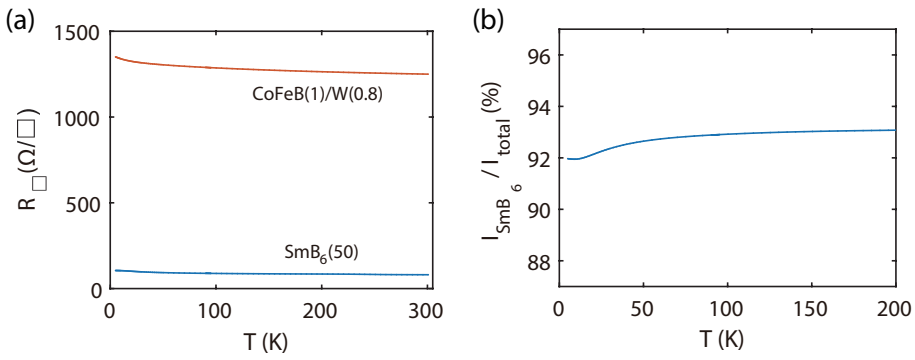

fig. S8. Temperature dependence of resistance of SmB_6 and CoFeB/W multilayers. **a,** temperature dependence of $R_\square$ of 50 nm-thick SmB_6 film (blue) and MgO(1.5)/CoFeB(1)/W(0.8) trilayer. **b,** I_{SmB_6}/I_{tot} for MgO(1.5)/CoFeB(1)/W(0.8)/SmB_6(50).

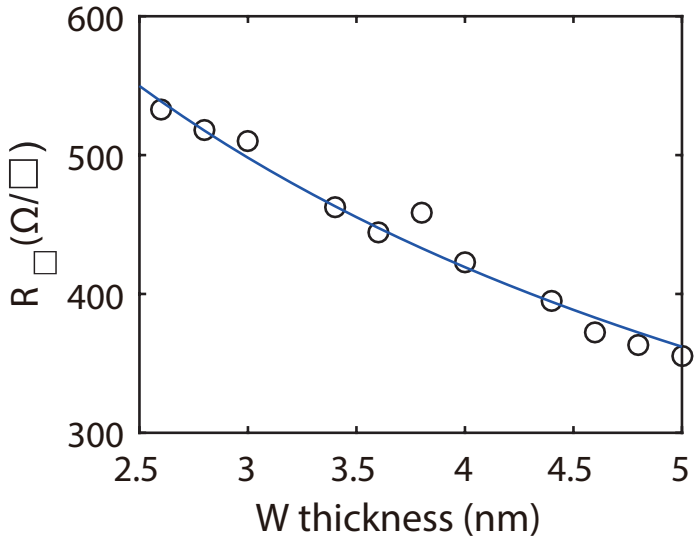

fig. S9. Sheet resistance of CoFeB/W multilayer as a function of W thicknesses. Sheet resistance of MgO(1.5)/CFB(1)/W(t) and fitting using two-coductor-in-parallel model (blue curve).

values [39, 40]. The high resistivity of W is usually taken as a signature of β phase. In our experiments, a protective 1 nm-thick Ta layer is capped on the magnetic trilayer to prevent it from oxidization. This capping layer is expected to oxidize in ambient pressure and do not contribute to electrical conductivity [39, 40]. We note that it will not affect the accuracy of our quantitative analysis even if the capping layer is not completely oxidized, in which case its potential contribution to the conductivity is either accounted for by the resistance of the trilayer when assessing I_{SmB_6}/I_{total}, or by ρ_{CFB} when assessing the current distribution in W.